Appl Magn Reson (2014) 45:517–525
DOI 10.1007/s00723-014-0537-3

Applied
Magnetic Resonance

Visualization and Quantification of Vascular Structure of Fruit Using Magnetic Resonance Microimaging

Satoshi Moriwaki · Yasuhiko Terada · Katsumi Kose · Tomoyuki Haishi · Yoshihiko Sekozawa

Received: 17 December 2013 / Revised: 28 March 2014 / Published online: 13 April 2014

Abstract Three-dimensional magnetic resonance (MR) images of four kinds of fruit (Japanese apricot, peach, Japanese pear, and apple) were acquired throughout their growing periods (from April to August) to visualize and quantify their vascular structures. The vascular structures were emphasized using T_1-weighted spin-echo or gradient-echo pulse sequences, visualized using a maximum-intensity projection technique, and quantified using an image-segmentation program. As a result, we demonstrated that the vascular volume changed almost in proportion to the whole volume and that larger fruits generally had larger proportionality constants. We therefore concluded that MR microimaging is a powerful tool for studies of the vascular structure of fruit.

1 Introduction

Vascular bundles in fruit are essential for transport of water and nutrients. The visualization and evaluation of the vascular bundles are indispensable for understanding the development and growth of fruit.

Currently, the standard method for visualization of the vascular bundles in fruit is chemical fixation, slice sectioning, staining, and observation using an optical microscope [1]. However, the standard method is destructive, time consuming, and

S. Moriwaki · Y. Terada · K. Kose (✉)
Institute of Applied Physics, University of Tsukuba, 1-1-1 Tennodai, Tsukuba 3058573, Japan
e-mail: kose@bk.tsukuba.ac.jp

T. Haishi
MRTechnology Inc, 2-1-6 B5 Sengen, Tsukuba 3050047, Japan

Y. Sekozawa
Agricultural and Forestry Research Center, University of Tsukuba, 1-1-1 Tennodai, Tsukuba 3058577, Japan

not appropriate for three-dimensional (3D) visualization. High-resolution X-ray computed tomography (CT) can be used for 3D visualization of vascular bundles, but some contrast enhancement method using heavy elements for the vascular tissues is indispensable because plant tissues mostly consist of light elements with low X-ray absorptions [2–4].

In contrast, magnetic resonance imaging (MRI) or magnetic resonance microimaging (MR microimaging), which is high-resolution MRI with a few to 100 μm spatial resolution, can be a useful method for 3D visualization and quantification of the vascular structure in fruit without any contrast agents. This works well in fruit because the relaxation times of water protons in the vascular bundles and those in the surrounding tissue are substantially different [5, 6]. In addition, MRI is also useful for vascular tissue functioning studies [7].

In this study, 3D vascular structures in four kinds of fruit, two kinds of 'true fruit,' and two kinds of 'accessory fruit,' were visualized and their volumes were quantified in the growing process using 3D MRI sequences to demonstrate the usefulness of MR microimaging in studies of fruit.

2 Materials and Methods

2.1 Fruit Samples

Fruit samples of Japanese apricot 'Nanko' (*Prunus mume. Sieb. et Zucc.*), peach 'Hikawa-Hakuhou' (*Prunus persia L.*), Japanese pear 'Kousui' (*Pyrus pyrifolia* Nakai var. *culta* Nakai), and apple 'Tsugaru' (*Malus pumila*) were collected every week from the period of floral abscission to that of harvest in a research orchard in the Agricultural and Forestry Research Center of the University of Tsukuba. The sampling periods were actually from April 10 to June 27 for the Japanese apricot, from May 16 to July 4 for the peach, from May 2 to August 23 for the Japanese pear, and from May 16 to August 19 for the apple in 2013.

The Japanese apricot and peach fruits are categorized as true fruit, whereas the Japanese pear and apple fruits are categorized as accessory fruit. The edible part of the true fruit is derived from a ripened ovary and that of the accessory fruit is derived from a receptacle, the thickened part of a peduncle. The fruit samples were wrapped with a food wrapper just after sampling to prevent them from drying during the MR microimaging measurements. The measurements were performed at room temperature within a week after sampling.

2.2 MR Microimaging Measurements

Two MRI systems with different room-temperature bore size (88.3 and 280 mm) magnets were used for 3D MR microimaging measurements of the fruit samples. The small-bore system uses a vertical bore superconducting magnet (field strength = 4.74 T, resonance frequency of protons = 202 MHz) with a digital MRI console (MRTechnology, Tsukuba, Japan) [8]. The large bore system uses a horizontal bore superconducting magnet (field strength = 1.1 T, resonance

frequency of protons = 46.8 MHz) with an analog MRI console (MRTechnology). Six gradient coil probes consisting of planar gradient coil sets, radio frequency (RF) shielding boxes, and solenoid RF coils, optimized for the signal-to-noise ratio (SNR) of MR images of the fruit samples, were used with the superconducting magnets [9]. The open diameters of the gradient coil probes ranged from 13 to 96 mm and their specifications are detailed in Table 1.

The fruit samples with diameters ranging from 8 (minimum) to 39 mm were measured with the vertical bore MRI system using a 3D spin-echo (3DSE) sequence [image matrix = 512 × 256 × 256, repetition time (TR) = 200 ms, echo time (TE) = 14 ms, number of excitations (NEX) = 4, total image acquisition time = 14.6 h]. Fruit samples with diameters from 43 to 94 mm (maximum) were measured with the horizontal bore MRI system using a 3DSE sequence (image matrix = 256 × 256 × 256, TR = 200 ms, TE = 14 ms, NEX = 4, total image acquisition time = 14.6 h) and 3D gradient-echo sequence (image matrix = 256 × 256 × 256, TR = 100 ms, TE = 3.5 ms, NEX = 10, total image acquisition time = 18.2 h). To extend the dynamic range of the receiver of the horizontal bore system, a gain stepping scan technique was used [10–12]. Using this technique, the MRI signal data were acquired with a low gain (0 dB) in the central region of the k-space and with a high gain (+20 or +30 dB) in the high spatial-frequency region of the k-space. When the gain stepping scan was used, the total image acquisition time was elongated by several tens of minutes.

To clarify T_1 and T_2 dependence of the image intensity in a Japanese apricot sample, several 3D spin-echo images were acquired with different TR and TE values (TR/TE = 200 ms/14 ms, 800 ms/14 ms, 1,600 ms/14 ms, 800 ms/14 ms and 800 ms/64 ms). The matrix size for these experiments was 512 × 256 × 128.

2.3 Image Processing

For visualization of the vascular structures of the fruit samples, the maximum-intensity projection (MIP) technique was used after the high-intensity part of the fruit surface was removed using a home-built computer program. For quantification of the vascular and whole volume of the fruit samples, a medical-image segmentation software program (ITK-SNAP) was used [13]. Because the image-intensity distribution was not homogeneous over the 3D MR images, the threshold

Table 1 Specifications of the gradient coil probes

Open diameter (mm)	Number of RF coil turns	Efficiency, Gx (mT/m/A)	Efficiency, Gy (mT/m/A)	Efficiency, Gz (mT/m/A)
13	3	34.4	30.4	67.5
25	6	18.8	16.9	23.4
30	6	13.9	13.1	15.5
40	6	7.0	5.4	9.2
68	6	2.97	2.63	3.77
96	8	2.07	2.07	3.70

for the image intensity that differentiates that of the vascular bundle and that of the surrounding tissue was determined separately for several regions using the image-processing software, Image-J [14].

3 Results

3.1 T_1 and T_2 Dependence of the Image Intensity

Figure 1 shows T_1- and T_2-weighted images of a cross-section selected from 3D datasets of the Japanese apricot sample harvested on June 13. As shown in Fig. 1, large vascular bundles are visualized in both images but smaller vascular bundles are visualized only in the T_1-weighted image. The contrast mechanism will be discussed in the later section.

3.2 Visualization of Vascular Structures

Figure 2 shows MIP images calculated from T_1-weighted 3D images of the Japanese apricots (Fig. 2a, b), the peaches (Fig. 2c, d), the Japanese pears (Fig. 2e, f), and the apples (Fig. 2g, h). The samples shown in the left column (Fig. 2a, c, e, g) were harvested in the early stage and those in the right column (Fig. 2b, d, f, h) were harvested in the late stage of the growing process. As shown in the images, large vascular bundles start from the stems, branch into smaller vascular bundles, and reach close to the epidermis. Meanwhile, the large vascular bundles surround the seeds and some of them reach the seeds. A clear difference between the vascular structures of the true fruit and those of the accessory fruit is not present.

3.3 Image Segmentation and Volume Measurements

Figure 3 shows 3D-rendered segmented images of the vascular bundle and seeds (Fig. 3a), seeds (Fig. 3b), and vascular bundle (Fig. 3c) of a Japanese pear fruit sample. Because the image intensity for the seeds and the vascular bundle was nearly identical, they could not be differentiated by the image intensity. However, because the seeds were

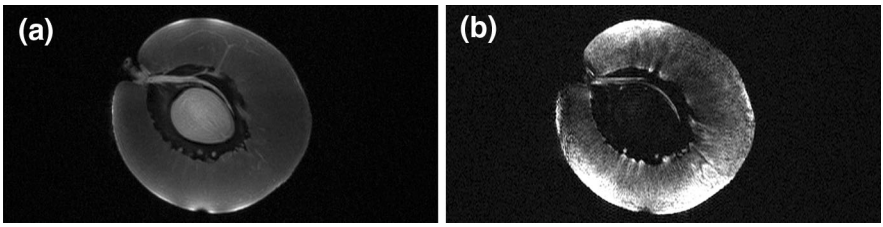

Fig. 1 T_1-weighted (**a**) and T_2-weighted (**b**) images of a Japanese apricot sample acquired at 4.7 T. The T_1-weighted image was acquired using a 3D spin-echo sequence with TR = 200 ms and TE = 14 ms. The T_2-weighted image was acquired using a 3D spin-echo sequence with TR = 800 ms and TE = 64 ms. The vascular bundle is clearly differentiated from the surrounding tissues using the T_1-weighted image

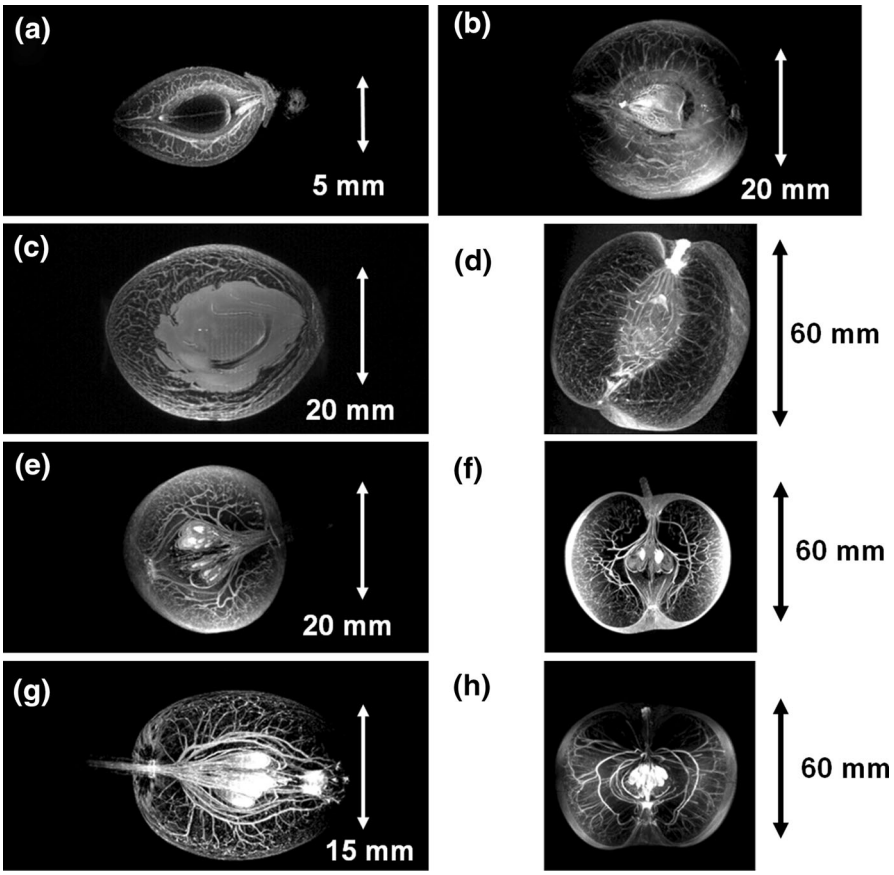

Fig. 2 MIP images calculated from T_1-weighted 3D images of the Japanese apricot (**a**, **b**), the peach (**c**, **d**), the Japanese pear (**e**, **f**), and the apple (**g**, **h**). **a** Harvested on April 10. In-plane resolution: 60 μm. **b** Harvested on May 23. In-plane resolution: 160 μm. **c** Harvested on May 30. In-plane resolution: 160 μm. **d** Harvested on June 27. In-plane resolution: 260 μm. **e** Harvested on May 30. In-plane resolution: 160 μm. **f** Harvested on July 25. In-plane resolution: 400 μm. **g** Harvested on May 15. In-plane resolution: 100 μm. **h** Harvested on August 8. In-plane resolution: 400 μm

localized, their visualization was possible using a region growing technique. The volume of the vascular bundle was measured after the seeds were removed from the 3D-rendered segmented images for all fruits and all stages of fruit growth.

3.4 Correlation Between the Whole Volume and the Vascular Volume

Figure 4 shows the variation over time of the whole volume and the vascular volume plotted against the harvest dates for the four kinds of fruit. As shown in Fig. 4, the vascular volume changes almost in proportion to the whole volume. Figure 5 shows correlations between the vascular volume and the whole volume for the four kinds of fruit. The correlation coefficients ranged from 0.964 to 0.991 and the coefficients of the first-order term for the linear regression equations ranged from 0.040 (Japanese

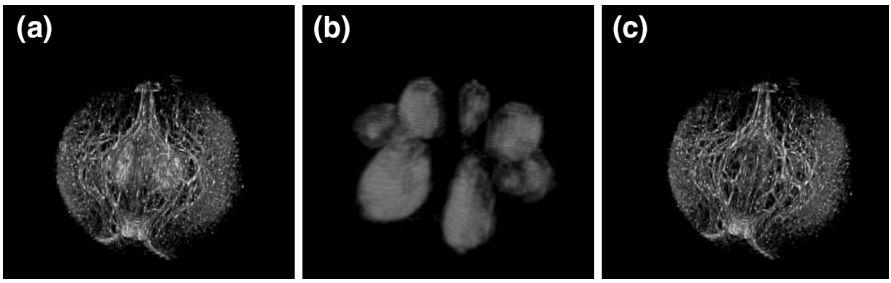

Fig. 3 **a** A 3D-rendered segmented image of the vascular and seed of the Japanese pear fruit. **b** A 3D-rendered segmented image of the seeds. **c** A 3D-rendered segmented image of the vascular bundles. The seed was removed

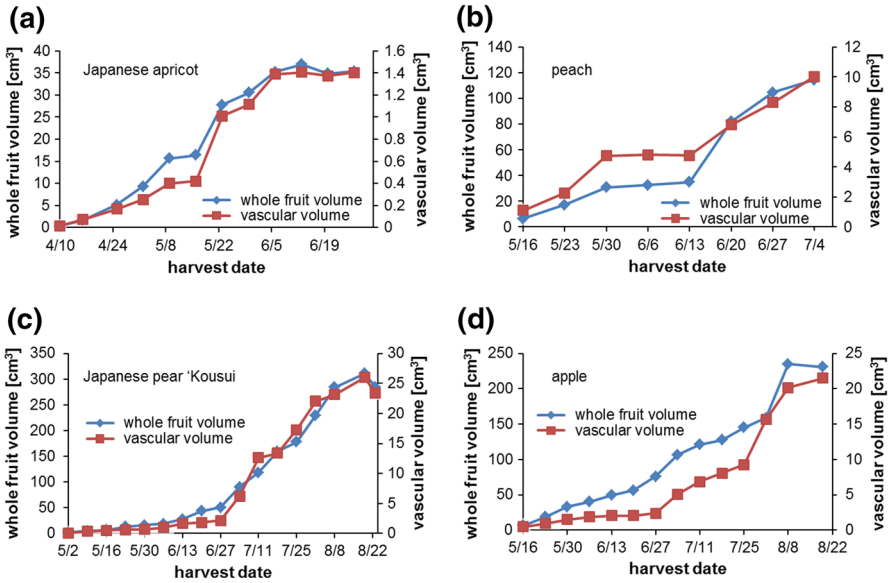

Fig. 4 Variation over time of the whole volume and the vascular volume plotted against the harvest dates for the four kinds of fruit: **a** Japanese apricot, **b** peach, **c** Japanese pear, **d** apple

apricot) to 0.094 (apple). We cannot find a clear difference between true and accessory fruits for the structure and volume of the vascular bundles. However, in general, larger fruits have a larger vascular volume proportion.

4 Discussion

4.1 Image Contrast for Vascular Segmentation

As shown in Fig. 1, the T_1-weighted image can clearly visualize the vascular bundles of the Japanese apricot. Although the relaxation time-weighted images were

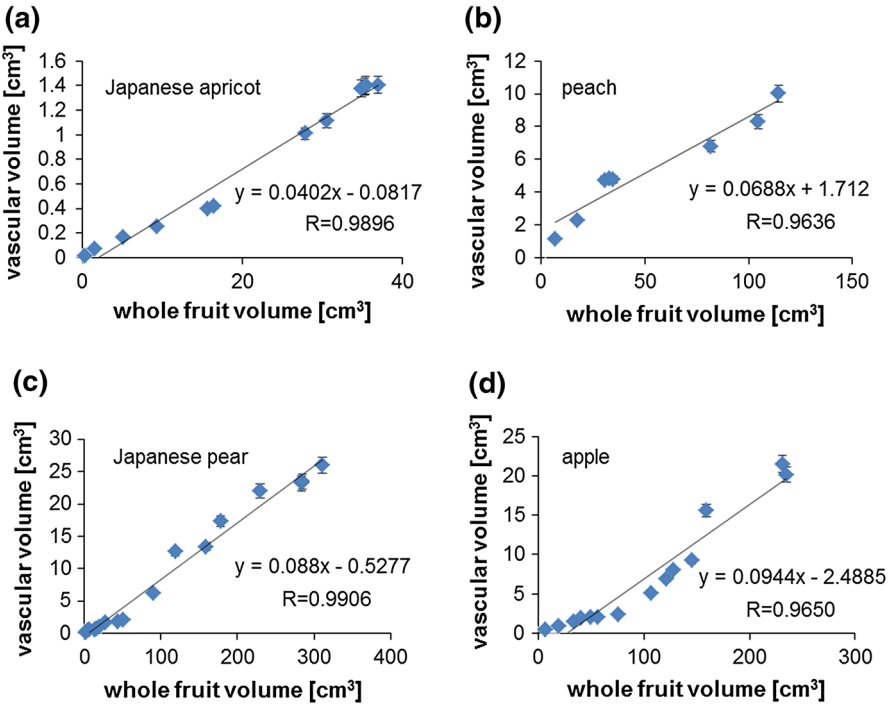

Fig. 5 Correlations between the whole volume and the vascular volume for the four kinds of fruit: **a** Japanese apricot, **b** peach, **c** Japanese pear, **d** apple

measured only for the Japanese apricot, the same contrast mechanism is expected for the other fruit as shown in Fig. 2. This is because the shortening of T_1 and T_2 of the protons in the vascular bundle is partly caused by surface relaxation of the mobile water protons [15–17], which originates from the fact that the cell size of the vascular bundle is much smaller than that of the surrounding tissue. There are various kinds and sizes of membranes in the fruit tissues, but as a whole, T_1 and T_2 relaxation are accelerated on the membrane more in the vascular bundles than in the surrounding tissues.

Although various mechanisms for the difference of the relaxation times between the vascular bundles and the surrounding tissues can be conceived, it is important that we succeeded in visualizing the vascular bundles as high contrast regions using the T_1-weighted sequence throughout the growing stages for all the fruits used in this study.

4.2 Accuracy of the Image Segmentation

It is well known that image quantification (e.g., volume) based on image segmentation is sensitive to the threshold used for the segmentation of the specified regions. In this study, we evaluated errors in the volume measurements by repeatedly changing the threshold for the image segmentation. As a result, we

confirmed about 10 % fluctuation in the volume measurements. Because the segmentation error depends on the contrast-to-noise ratio (CNR) of the segmented regions in the MR image, it is essential to achieve a sufficient CNR (>10) for the vascular bundles.

4.3 Spatial Resolution

The most serious limitation of MR microimaging in visualization of the vascular structure is spatial resolution. The spatial resolution in MR microimaging is ultimately limited by the SNR per voxel, if sufficient magnetic field gradient strength is available. For a certain sample, the SNR per voxel is determined by the magnetic field strength, B ($SNR \propto B^{7/4}$) [18], the sensitivity of the RF coil ($SNR \propto \sim R^{-1}$, R: coil radius), the frequency bandwidth, BW, per voxel ($SNR \propto BW^{-1/2}$), NEX ($SNR \propto NEX^{1/2}$), and the efficiency of the pulse sequence. In this study, we used two superconducting magnets (4.74 and 1.1 T), solenoid RF coils optimized for the sample size, reasonable frequency bandwidth (195 Hz/voxel), reasonable total measurement times (about 15–20 h) for the fruit samples, and T_1-weighted sequences with 200 ms repetition time. Although much higher magnetic fields (e.g., 9.4 T or higher) may be available, we think that our MRI systems are optimized for visualization of vascular structures of fruit and have sufficient capability.

4.4 Detectability of the Vascular Structure

As MRI traces only water-filled vessels, then the vascular volume has to be measured on the fresh well watered fruits. Therefore, the above discussion and our conclusion are valid for the water-filled vessels.

5 Conclusion

T_1-weighted 3D MR images of four kinds of fruit were acquired throughout the growing process and their vascular structures were visualized and quantified. As a result, it was demonstrated that the vascular volume changed almost in proportion to the whole volume of the fruit and it was observed that larger fruits generally had larger proportionality constants. We therefore concluded that MR microimaging is a powerful tool for studies of vascular structures of fruit.

Acknowledgments We thank Dr. Sumiko Sugaya for valuable advice on this study and Mr. Daiki Tamada for valuable help with image processing.

References

1. N. Feder, T.P. O'Brien, Am. J. Bot. **55**, 123–142 (1968)
2. C.R. Brodersen, E.F. Lee, B. Choat, S. Jansen, R.J. Phillips, K.A. Shackel, A.J. McElrone, M.A. Matthews, New Phytol. **191**, 1168–1179 (2011)

3. O. Leroux, J.P. Knox, B. Masschaele, A. Bagniewska-Zadworna, S.E. Marcus, M. Claeys, L. van Hoorebeke, R.L.L. Viane, Ann. Bot. **108**, 307–319 (2011)
4. Y.M. Staedler, D. Masson, J. Schönenberger, PLoS One **8**(9), e75295 (2013)
5. B. Williamson, B.A. Goodman, J.A. Chudek, G. Hunter, J.A.B. Lohman, New Phytol. **128**, 39–44 (1994)
6. C.J. Clark, J.S. MacFall, Magn. Reson. Imaging **21**, 679–685 (2003)
7. J. Van As, Exp. Bot. **58**, 743 (2007)
8. S. Hashimoto, K. Kose, T. Haishi, Rev. Sci. Instrum. **83**, 053702 (2012)
9. M. Horiga, K. Ishizawa, K. Kose, Proc. Int. Soc. Magn. Reson. Med, p. 2712 (2013)
10. K. Kose, K. Endoh, T. Inouye, IEEE Aerosp. Electron. Syst. Mag. **5**, 27–30 (1990)
11. M.A. Elliott, E.K. Insko, R.L. Greenman, J.S. Leigh, J. Magn. Reson. **130**, 300–304 (1998)
12. R. Behin, J. Bishop, R.M. Henkelman, Concepts Magn. Reson Part B **26B**, 28–35 (2005)
13. P.A. Yushkevich, J. Piven, H.C. Hazlett, R.G. Smith, S. Ho, J.C. Gee, G. Gerig, Neuroimage **31**, 1116–1128 (2006)
14. http://rsb.info.nih.gov/ij/. Accessed 10 Apr 2014
15. K.R. Brownstein, C.E. Tarr, Phys. Rev. **A19**, 2446–2453 (1979)
16. L. van der Weerd, M.M.A.E. Claessens, T. Ruttink, F.J. Vergeldt, T.J. Schaafsma, H. Van As, J. Exp. Bot. **52**, 2333–2343 (2001)
17. Y. Geya, T. Kimura, H. Fujisaki, Y. Terada, K. Kose, T. Haishi, H. Gemma, Y. Sekozawa, J. Magn. Reson. **226**, 45–51 (2013)
18. D.I. Hoult, R.E. Richards, J. Magn. Reson. **24**, 71–85 (1976)